MJFAS
Malaysian Journal of Fundamental and Applied Sciences

Mohd Rozi *et al.* | Malaysian Journal of Fundamental and Applied Sciences, Vol. 21 (2025) 2032-2044

RESEARCH ARTICLE

Garcinia mangostana Pericarp-Assisted Silver Nanoparticles as a Sustainable Solution for Tetracycline Contaminants Removal from Wastewater

Nurshahira Mohd Rozi[a], Sheela Chandren[a,b], Norazah Basar[a]*

[a]Department of Chemistry, Faculty of Science, Universiti Teknologi Malaysia, 81310 UTM Johor Bahru, Johor, Malaysia; [b]Centre for Sustainable Nanomaterials, Ibnu Sina Institute for Scientific and Industrial Research, Universiti Teknologi Malaysia, 81310 UTM Johor Bahru, Johor, Malaysia

Abstract To date, research endeavours are progressively oriented toward uncovering sustainable approaches for synthesizing metal nanoparticles. Biosynthesis methods involving plants have emerged as a viable alternative to foster environmental sustainability. This study explores a one-pot and room-temperature method for synthesizing silver nanoparticles (AgNPs) using agricultural waste, *Garcinia mangostana* pericarp (GMP), to degrade tetracycline cost-effectively. High-performance liquid chromatography (HPLC) detected the presence of α-mangostin, suggesting a dual-functioning agent in reduction and stabilization in the green synthesis. Ultraviolet-visible spectroscopy (UV-Vis) monitored stable colloid formation and revealed that the formation of AgNPs depends on molar ratio and pH. The optimal conditions for this single-step biosynthesis are: a molar ratio of extract to silver nitrate at 1:31, a basic environment with the extract at pH 10, and an incubation time of 2 hours. The successfully biosynthesized AgNPs were characterized using Fourier transform infrared (FTIR) spectroscopy, X-ray diffraction (XRD), field emission scanning electron microscope with energy dispersive X-ray (FESEM-EDX), and high resolution-transmission electron microscope (HR-TEM). The characterization unveiled the synthesis of uniformly spherical-shaped and mono-dispersed AgNPs with a size range of 8 to 22 nm and an Ag mass percentage of 65.5%. X-ray diffraction analysis confirmed the synthesized nanoparticle's face-centered cubic (FCC) crystalline nature with the (111) plane as the dominant peak. The photocatalytic performance of AgNPs was evaluated through the removal of tetracycline under ultraviolet (UV) light. The biosynthesized AgNPs demonstrated a degradation rate of 79%, with a constant rate 33 times greater than just by photolysis. These findings indicate that the plant-mediated biosynthesis of AgNPs is a promising photocatalyst for environmental remediation against tetracycline contaminants.

Keywords: *Garcinia mangostana*, biosynthesis, silver nanoparticles, photocatalytic, tetracycline.

***For correspondence:**
norazahb@utm.my

Received: 29 Aug. 2024
Accepted: 13 May 2025

Introduction

Nanotechnology refers to research and development of technology at the nanoscale, primarily focusing on materials with a size range of 1 to 100 nm [1]. Over the past few decades, nanotechnology as an emerging scientific field has experienced a rapid evolution due to the development of nanoparticles (NPs). NPs exhibit good catalytic, optical, electrical, and biological properties, thereby rendering them valuable across various applications. Noble metal NPs consist of metals such as gold, platinum, palladium, silver, and zinc. Among them, silver nanoparticles (AgNPs) have garnered significant attention in the scientific community due to the discovery of their unique properties. In the domain of metal NPs, AgNPs hold widespread applicability across fields from electronics to environmental remediation. AgNPs was found to enhance the performance of electrically conductive adhesives [2]. Additionally, AgNPs have proven effective as antimicrobial agents, combating bacteria such as *Escherichia coli* [3]. Furthermore,

research has proven that AgNPs are exceptional catalysts in accelerating the degradation of certain organic pollutants [4].

The synthesis of AgNPs can be accomplished using various techniques such as conventional and biological methods. Previously, conventional methods such as chemical reduction, chemical vapour deposition, laser ablation, and sputtering were extensively used for metal nanoparticle synthesis which were categorized into physical and chemical reduction methods [5]. These conventional methods were preferred for their capacity to produce large-scale nanoparticles at precise sizes in a short amount of time. However, the drawback of these conventional methods lies in the production of toxic by-products, prolonged processing time, and high cost. The toxicity issue in chemical reduction methods arose from using hazardous reducing agents like sodium borohydride ($NaBH_4$) that pose environmental risks [6]. Furthermore, chemical vapour deposition is less efficient due to its long processing time [6]. Meanwhile, the laser ablation and sputtering methods are costly as they require expensive equipments with high energy consumption [7]. Due to the multiple challenges and potentially hazardous effects associated with conventional methods for AgNPs synthesis. It is also essential to develop alternative approaches for synthesizing nanoparticles that are cost-effective and rely on eco-friendly, renewable resources such as phytochemical constituents from plants. As such, these factors result in a shift towards biosynthesis. This involved applying the principles of green synthesis as a rapidly evolving chemical science. Recent findings have highlighted the efficacy of various plants from *Bryophyllum pinnatum*, *Dracaena cochinchinensis*, *Hibiscus cannabinus L.*, *Dilenia indica*, and *Cannabis sativa*. *Moringa oleifera,* and *Eugenia roxburghii DC* in producing AgNPs [8-14]. These botanical sources contain bioactive compounds that plants use as reducing and capping agents in facilitating the biological conversion of metal ions into metallic nanoparticles [1].

Garcinia mangostana Linn (*G. mangostana*), a species of *Guttifeare* family, is a slow-growing evergreen tree with a pyramidal crown. Famously known as the '*mangosteen*' and hailed as the '*queen of fruits*' due to its tropical taste, the fruit of *G. mangostana* is a subglobose berry enveloped in a purple pericarp. It has 4-8 triangular segments of soft, juicy flesh with a mild acidic taste [15]. *G. mangostana* is cultivated widely in Southeast Asia, including Malaysia, Thailand, and Philippines [16]. Additionally, *G. mangostana* is a significant crop in Malaysia due to this region's ideal climate, which provides suitable humidity and temperature for growing this species. *G. mangostana* is renowned for its diverse pharmacological properties, such as anti-cancer, anti-inflammatory, anti-bacterial, and anti-oxidant [17-20]. The mangosteen shows a transitioning colour from yellowish-white to reddish-purple as it ripens. It is widely commercialized in the food industry as it is consumed freshly and processed into juice and jam [21]. Phytochemical exploration of *G. mangostana* has revealed that prenylated and oxygenated xanthones are promising secondary metabolites responsible for the diverse bioactivities exhibited by the plant [22]. Recently, *G. mangostana* was utilized as a reducing agent in the synthesis of AgNPs and demonstrated its efficacy as an inhibitory agent against *Pseudomonas aeruginosa* and *Staphylococcus aureus*, as well as its significant catalytic reduction of dyes like rhodamine B (RhB), methyl orange (MO), and 4-nitrophenol (4-NP) [6]. Despite these promising results, there remains a scarcity of research on biosynthesis using *G. mangostana*, specifically its bioactive compounds like α-mangostin as a major xanthone. This scarcity limits the exploration of its potential application in contamination remediation, especially concerning active pharmaceutical ingredients (APIs).

The pharmaceutical industry stands out as one of the pivotal industries contributing significantly to a country's economy. Despite the swift growth of the pharmaceutical industry, understanding of the global prevalence of pharmaceuticals in rivers is still limited. Global studies have detected a diversity of APIs that are inevitably released into rivers, lakes, and other water bodies during their production, utilization, and disposal [23]. The existence of APIs in aquatic environments carries ecological consequences, potentially influencing the reproductive process, disrupting endocrine systems, and contributing to the development of antibiotic-resistant bacteria. Aside from analgesic medications, antibiotics are one of the most widely manufactured pharmaceuticals. Tetracycline has gained notable prominence among the commonly used antibiotics attributed to its broad-spectrum effectiveness, affordability, and robust efficiency [24]. The human daily intake of tetracycline is estimated at 23 kg per day worldwide [25]. Consequently, the environmental and human health implications of excessive tetracycline usage have become a concern. This attracts the attention of researchers to develop a proper wastewater treatment process for restoring polluted environments.

Analysis of existing literature reveals a limited number of studies investigating agricultural waste's capability to synthesize AgNPs. The mangosteen pericarp, in particular, may potentially be utilized for AgNPs synthesis due to its high content of α-mangostin. Therefore, this study aimed to determine the optimal conditions for fast and economical production of AgNPs with maximum effectiveness in tetracycline removal by using *G. mangostana* pericarp (GMP). The parameters such as molar ratio of GMP:$AgNO_3$, pH of GMP extract, and incubation time were investigated. To the best of our knowledge,

available resources on the degradation of antibiotics using green AgNPs produced via the biosynthesis approach are still limited.

Materials and Methods

The materials used in this research were acetonitrile [HPLC grade], silver nitrate $AgNO_3$ [Sigma-aldrich (99.99%)], tetracycline [Sigma-aldrich (98.00%)], and absolute ethanol [HmBG (99.90%)]. All materials were used as-received without further purification. Deionized water was used throughout the experiments.

Preparation of Plant Extract

Fresh fruits of *G. mangostana* were collected from Kota Tinggi, Johor, Malaysia. The pericarp was pared, washed to remove the dust, and air-dried for a fortnight. The dried sample was cut into small pieces and ground into powder. About 10 g of powdered pericarp was mixed with 50 mL of deionized water. The mixture underwent further extraction using sonication, where it was placed in an ultrasonic bath at 20 kHz for an hour at 50 °C. The extract was filtered using Buchner funnel filtration twice for a refined solution. The GMP extract was stored in a dark bottle and refrigerated for further use.

Identification of α-mangostin

Determination of α-mangostin in the previously prepared GMP extract was carried out using high-performance liquid chromatography (HPLC). The GMP extract underwent freeze-drying to yield a crude extract. The stock solution (1 mg/mL) was then prepared by weighing 3 mg of GMP crude extract and dissolving it in 3 mL acetonitrile. Subsequently, the solution was filtered using a MILLEX 0.22 µm membrane filter. For analysis, Shimadzu LC-20ADXR with a photodiode array (PDA) detector equipped with an auto-sampler was employed under isocratic conditions. The Supelco Ascentis C-18 column (250 mm x 4.6 mm x 5 µm) was utilized and two mobile phases: A (20% deionized water) and B (80% acetonitrile), were pumped at a flow rate of 1.0 mL/min at room temperature. A 10 µL was used and the photodiode array was monitored at 243 nm. The chromatographic peak was confirmed by comparing its spectra and retention time with the reference standard.

Biosynthesis of Silver Nanoparticles

The biosynthesis of AgNPs involved mixing an aliquot of $AgNO_3$ with GMP extract as a capping and stabilizing agent. 1 mM $AgNO_3$ solution was prepared by stirring 16.9 mg of $AgNO_3$ in 100 mL of deionized water for one hour at room temperature. A sufficient amount of GMP extract reacted with 1 mM $AgNO_3$ solution at room temperature. Confirmation of AgNP formation was based on colour shifts to yellowish-dark brown and the presence of a broad peak at UV. The resulting colloidal solution underwent centrifugation at 4000 rpm for 30 min. The sediment was re-dispersed in deionized water and centrifuged again to eliminate impurities. The method was repeated twice. The resulting suspension was then dried in a vacuum oven overnight before analysis.

Biosynthesis Optimizing

To maximize the production of AgNPs and enhance their efficiency, various parameters have to be optimized. These parameters include the different molar ratios for GMP:$AgNO_3$ (1:11, 1:14, 1:17, 1:22, and 1:31), adjusting the pH of GMP extract (2, 4, 6, 8, and 10), and varying the incubation time (1 to 5 hours). The systematic optimization of these parameters will help to achieve the desired results of AgNP synthesis.

Characterization of Biosynthesized Silver Nanoparticles

The bio-reduction of the Ag^+ ions in the solution was monitored using UV-visible spectroscopy (UV-Vis) in quartz cuvettes with a double-beam spectrometer (Shimadzu UV-1610PC) in the 270–800 nm range. Identification of functional groups using Fourier-transform infrared spectroscopy (FTIR) was carried out by Perkin-Elmer Spectrum 1600 at 4000–500 cm^{-1} using the potassium bromide pressed disc method. The XRD patterns of dried NPs pellets were generated using a Rigaku X-ray diffractometer (SmartLab model) with Cu Kα radiation (λ = 1.5418 Å), operating at 30 mA and 40 kV. The average crystallite size of AgNPs was calculated using Debye-Scherrer in Equation (1):

$$D = \frac{K\lambda}{\beta \cos\theta} \quad (1)$$

where D is the crystallite size, K is the Scherrer's constant, λ is the Cu Kα wavelength, β is the full width at half maximum (FWHM) of the maximum intensity peak, and θ is the Bragg's diffraction angle.

Nanoparticle morphology was analysed through images obtained with a high-resolution transmission electron microscope (HRTEM JEOL JEM-2100) and field emission scanning electron microscope (FESEM JSM-6701F) equipped with energy dispersive X-ray (EDX) attachment. The polydispersity of the biosynthesized AgNPs was calculated using Equation (2). The specific pore size distribution was determined by multipoint Brunauer-Emmet-Teller (BET) analysis using Micromeritics ASAP 2020 using N_2 as adsorbed gas.

$$PDI = \frac{\sigma}{\mu} \text{ x } 100\% \quad (2)$$

where *PDI* is the polydispersity index, σ is the standard deviation, and μ is the average nanoparticle size.

Photocatalytic Activity of Biosynthesized Silver Nanoparticles

In this study, the degradation of tetracycline was chosen as the model to assess the photocatalytic performance of bio-synthesized AgNPs under UV light. AgNPs photocatalyst weighing 0.05 g was introduced into 60 mL of 30 ppm tetracycline solution. The solution was then placed in a box under a UV light source featuring a 6 W lamp from Vilder Lourmat and was continuously stirred using a magnetic stirrer. The reaction was conducted for 4 hr. At 20 min intervals throughout the reaction, 3 mL of the tetracycline solution was extracted, and its concentration was analysed using a UV-Vis spectrometer at a wavelength of 365 nm, which is a characteristic absorption for tetracycline. The degradation of tetracycline and rate constant (*k*) was calculated using the following formula stated in Equations (3) and (4), simultaneously.

$$\frac{C_i - C}{C_i} \text{ x } 100\% \quad (3)$$

where, C_i and C are the concentration of tetracycline after 1 hr in dark reaction and after UV exposure, respectively.

Equation (4) was used to measure the rate constant (*k*) for each sample.

$$\ln\frac{A}{A_0} = -kt \quad (4)$$

where, A and A_0 are the absorbance of tetracycline at a particular time interval and time 0, *k* is the rate constant and *t* is the reaction time.

Results and Discussion

Identification of α-mangostin

In this part, the potential of target α-mangostin involved in the biosynthesis of AgNPs is discovered. Isocratic elution was favoured over gradient elution due to its maximum loading capacity and faster separation speed [26]. Figures 1(a) and 1(b) illustrate the chromatogram of reference α-mangostin and the GMP crude extract, respectively. In Figure 1(a), an unambiguous and narrow peak appeared at 8.59 min, corresponding to α-mangostin. Meanwhile, Figure 1(b) revealed several peaks, with a prominent peak observed at 8.60 min. Hereby, the presence of α-mangostin in the GMP crude extract was validated by comparing the retention time with the reference peak. The α-mangostin present in the GMP extract, is classified within the category of polyphenolic compounds. Compounds containing phenols are recognized for their good reducing capabilities, making them valuable for the synthesis of metal nanoparticles [27].

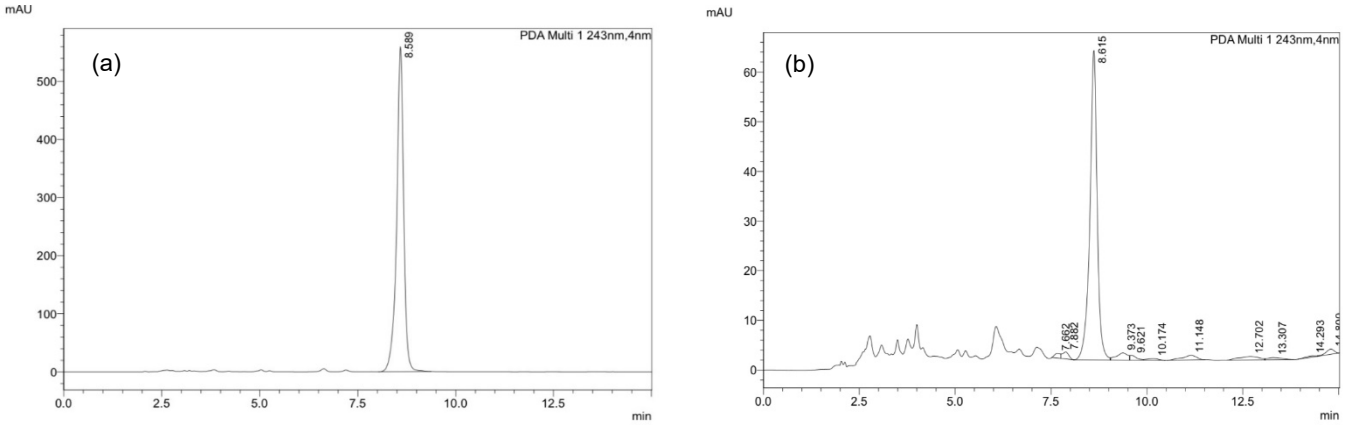

Figure 1. HPLC chromatograms of (a) α-mangostin and (b) *Garcinia mangostana* pericarp (GMP) extract

UV-Visible Spectroscopy Characterization

The UV-Vis analysis was conducted to observe the changes in reaction parameters including molar ratio, pH, and incubation time impact the biosynthesis of AgNPs. The absorption peak was assigned to the surface plasmon resonance (SPR) band of AgNPs, resulting from the collective oscillation of conduction electrons in the NPs by incident light [28].

Effect of Molar Ratio

In this optimization process, the incubation time of 24 hr and pH 6 were fixed. Different molar ratios were employed, thus leading to the observation of a broad peak in UV spectroscopy. Figure 2(a) illustrates the SPR bands ranging between 420 to 450 nm. The change in solution colour from light yellow to dark brown represents a common characteristic of AgNPs biosynthesis. Based on Figure 2(b), positive changes in colour were observed for all solutions after 24 hr, suggesting the occurrence of a reduction reaction. These colour changes result from the strong absorption of visible light induced by the excitation of surface plasmon in the nanoparticles [29]. Notably, the reaction mixture with GMP:$AgNO_3$ of 1:31 exhibited a rapid and intense darkening and also the highest intensity of SPR compared to the other molar ratios. The UV-Vis peak is more prominent with a higher volume of $AgNO_3$, indicating the formation of a greater amount of nanoparticles per unit volume at this particular rate [30].

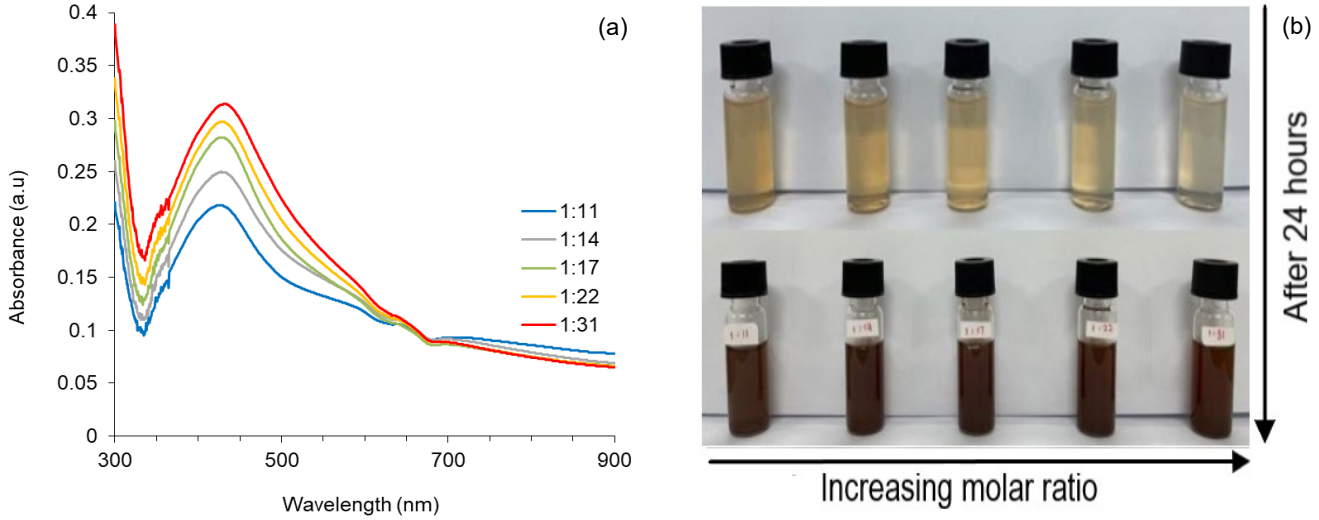

Figure 2. Optimization on GMP:$AgNO_3$ molar ratio demonstrated by (a) UV-Vis spectra of the reaction and (b) colour transition of colloidal Ag after 24 hours

Effect of pH

The critical function of the pH value of aqueous extract was emphasized in the synthesis of AgNPs through the incorporation of GMP. The absorption spectra of colloidal Ag influenced by the pH, are illustrated in Figure 3(a). A noticeable colour transformation of colloidal Ag was observed in Figure 3(b) with varying pH values from 2 to 10. The solution displayed a faint purplish-pink colour at pH 2 and 4, transitioning from a clear to pale orange shade at pH 6. Meanwhile, an intense yellow-brownish colour reflected at pH 8 and 10. This corresponded with UV-Vis spectra at different pH values revealing the initiation of the SPR band and enhancement of absorption intensity starting at pH 6. The detected maximum peaks at pH 6, 8, and 10 exhibited blue shifts around 438, 425, and 420 nm, respectively. This phenomenon suggests a reduction in the size of nanoparticles with increasing pH [31]. The difference in λ_{max} indicates the difference in size and shape of AgNPs [32]. The absence of SPR bands at pH 2 and 4 is due to the electrostatic repulsions between H^+ and $AgNO_3^-$, which resulted in a gradual and less efficient reduction process as reported in the previous study [33]. In contrast, AgNP formation has proved favourable in an alkaline environment due to the ionization of functional groups such as OH^- on the AgNPs' surface, which also helps prevent agglomeration as a capping agent [34-35]. However, due to the correlation between higher pH levels and the formation of larger and non-uniform particles, this study was concluded at pH 10.

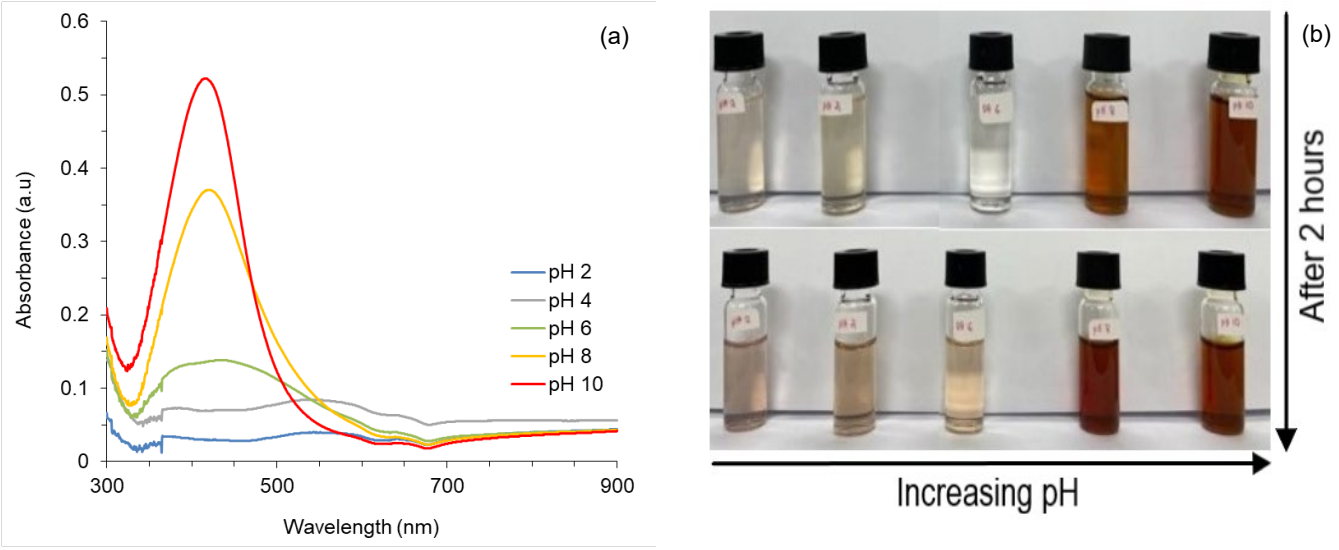

Figure 3. Optimization on pH of GMP extract demonstrated by (a) UV-Vis spectra of the reaction and (b) colour transition of colloidal Ag with increasing pH after 2 hours

Effect of Incubation Time

Following the optimization of the GMP to $AgNO_3^-$ molar ratio and the GMP pH, the impact of incubation time at various intervals was conducted and shown in Figures 4(a) and 4(b). It was observed that a slight adjustment in absorption intensity occurred with an extension of the reaction time up to 5 hr. Additionally, the SPR peak exhibited stability within the range of 420 to 428 nm, indicating the absence of blue or redshifts. Notably, the colloidal solution maintained its colour consistency from 2 to 5 hr, with no observable changes. Recently, a study focused on the usage of *G. mangostana* for AgNP synthesis stated that the silver nitrate solution required 3 hr for the colour to change from colourless to deep brown [36]. In contrast, this study observed a rapid change to a yellow-brownish colour within 2 hr. Consequently, an incubation time of 2 hr was considered optimal for synthesizing AgNPs. This highlights that once the reaction attains an optimal state, the incubation time halts to be a critical parameter.

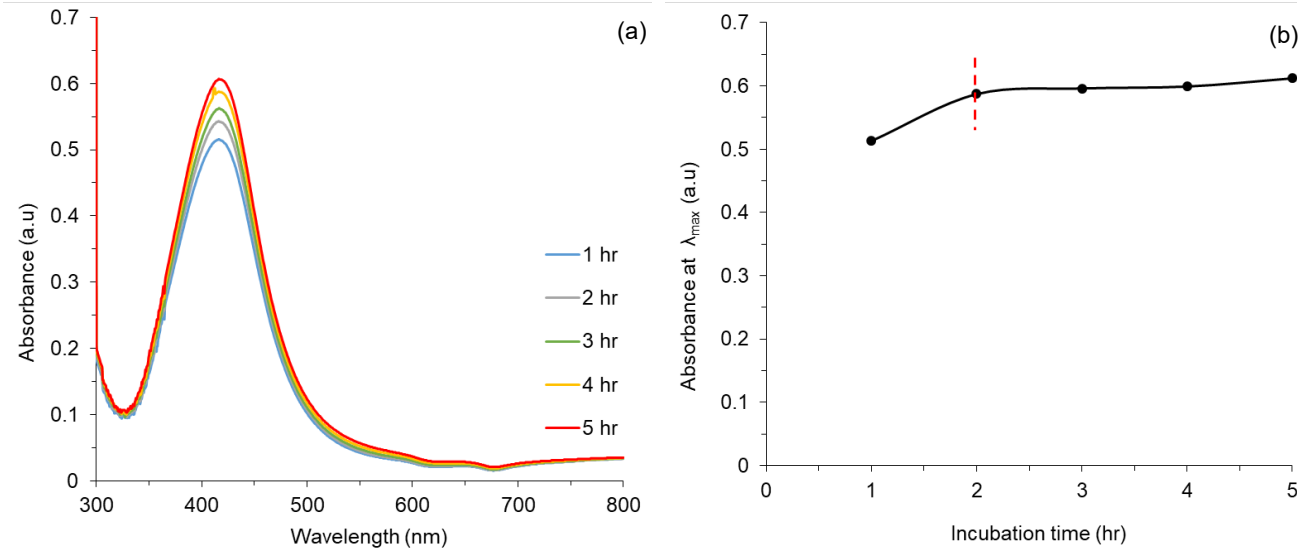

Figure 4. Optimization on incubation time demonstrated by (a) UV-Vis spectra of the reaction of colloidal Ag and (b) plot of maximum absorbance as a function of time

Functional Groups Determination

In this study, FTIR was employed to identify the functional groups within GMP extract accountable for the conversion of Ag^+ to Ag^0 atoms. According to Figure 5(a), the GMP extract spectrum revealed major peaks in the absorption band at 3255 cm^{-1} (–OH), 2964 and 2925 cm^{-1} (C-H), 1611 and 1455 cm^{-1} (C=C), 1643 cm^{-1} (C=O), and 1281 cm^{-1} (C-O). The depicted spectrum of biosynthesized AgNPs in Figure 5(b) illustrates an obvious decrease in the intensity of the bands within the fingerprint region around 600-1400 cm^{-1} after the introduction of $AgNO_3$ into GMP extract. This reduction strongly indicates the completion of AgNP synthesis and signifies the removal of GMP extract as a precursor in the process. The absorption band at 3425 cm^{-1} is attributed to the hydroxyl group that provides electrons for the reduction of Ag ions [33]. Additionally, this band broadened as the –OH group from the extract became bound to the surface of synthesized AgNPs, indicating intermolecular hydrogen bonding around AgNPs [37]. The peak observed around 2800 – 2980 cm^{-1} corresponds to C-H stretching present in the bi-product of GMP extract [38]. A peak at 2368 cm^{-1} was assigned to –CN stretching, as stated by Perera et al. [39]. The oxidation of the C-O bond (1281 cm^{-1}) to C=O results in a broad peak at 1615 cm^{-1}, coinciding with the reduction of Ag^+. A narrow peak at 1384 cm^{-1} suggests the binding of silver ions with carboxylate groups from GMP extract [40]. Furthermore, the narrow peak also corresponds to C-H symmetric vibration, a feature present in GMP extract [41]. The FTIR findings show the pivotal role of functional groups in GMP extract, contributing to the reduction and capping of green synthesized AgNPs.

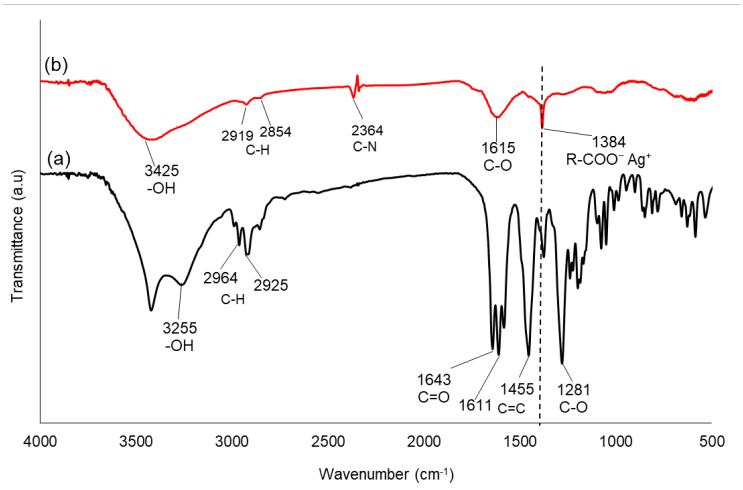

Figure 5. FTIR spectra of the (a) GMP extract and (b) biosynthesized AgNPs recorded in the range of 4000 to 500 cm^{-1}

X-ray Crystallography Analysis

X-ray diffraction (XRD) was used to determine the crystal structure of the AgNPs synthesized using GMP extract. The XRD measurement followed the Bragg-Brentano geometry, allowing for the investigation of the crystal nanostructure of the AgNPs. Figure 6 displays the XRD diffractogram of the biosynthesized AgNPs. The prominent peak confirms the polycrystalline nature of the synthesized AgNPs and ensures the face-centered cubic (FCC) structure [42]. The four diffraction peaks at 2θ values were observed around 38.10, 44.29, 64.42, and 77.37°. By referencing Bragg reflections and Miller indices (*hkl*), these peaks were identified and corresponding to the (111), (200), (220), and (311) crystallographic planes, respectively (reference: Joint Committee on Powder Diffraction Standards, JCPDS file No. 04-0783). The size of AgNPs on the intense (111) plane is measured at 8.96 nm, whereas the average crystallite size of AgNPs was calculated to be 14.24 nm using Debye-Scherrer equation.

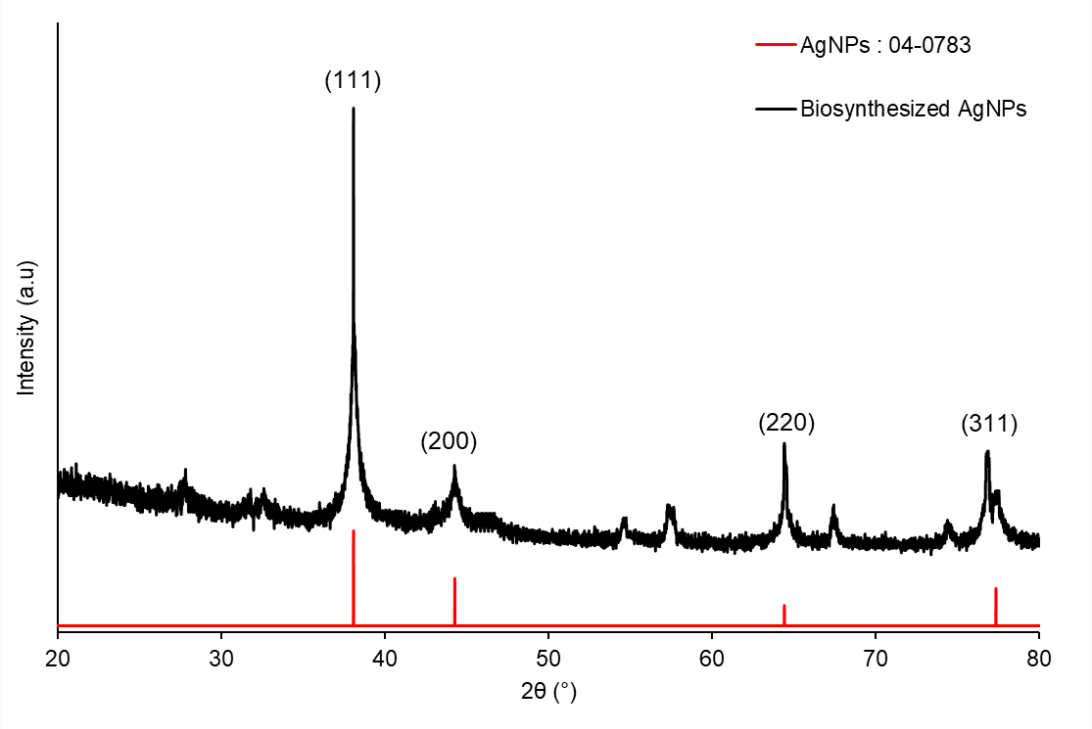

Figure 6. XRD diffractogram of biosynthesized AgNPs following JCPDS file No. 04-0783

Morphological and Elemental Analysis

FESEM-EDX and HR-TEM analyses were subsequently performed to determine the size, structure, and morphology of the AgNPs incorporated with GMP extract as a capping and stabilizing agent. The diverse sizes of nanoparticles were investigated at different magnifications, specifically 500 and 300 nm, as depicted in Figures 7(a) and 7(b), respectively. The results revealed that the biosynthesized AgNPs represented an almost spherical morphology with aggregations. The observation of larger particles attributed to agglomeration, given the high surface tension of ultrafine AgNPs [43]. To assess the purity of the synthesized AgNPs, EDX analysis was conducted to provide a semi-quantitative elemental analysis of Ag atoms in the study. As illustrated in Figure 7(c), the EDX analysis depicts a strong signal in the Ag region at approximately 3 keV, validating the presence of AgNPs with a mass percentage of 65.5%. The Ag metal exhibits a typical optical absorption peak between 2 to 4 keV due to SPR [44]. Additionally, other signals were detected, originating from elements in the *G. mangostana* pericarp as a starting material involved in stabilizing AgNPs [45].

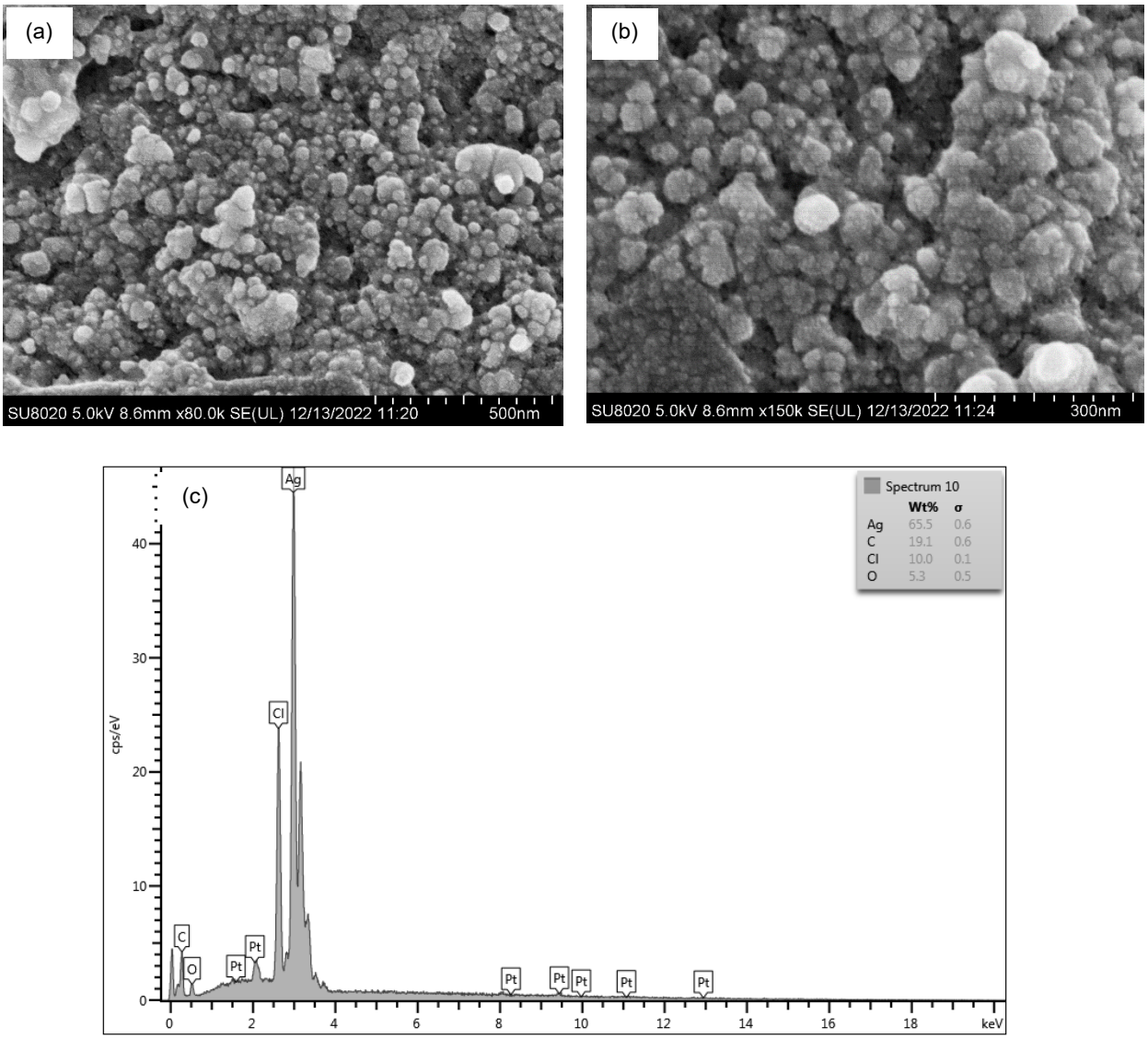

Figure 7. FESEM imaging at different magnifications (a) 500 nm; (b) 300 nm and (c) elemental mapping of biosynthesized AgNPs

For better clarification, HR-TEM was employed to provide insight into the size characteristic of AgNPs. The HR-TEM images presented in Figures 8(a) and 8(b) illustrate selected regions at different magnifications. In Figure 8(a), the image reveals dispersed spherical nanoparticles and agglomeration of smaller particles, confirming the findings obtained by FESEM. The size range of synthesized AgNPs is determined to be between 8–22 nm, with an average nanoparticle size of 13.42 nm. Figures 8(c) and 8(d) display images of high-resolution TEM along with its corresponding FFT plot and SAED pattern. The observed d-spacing of AgNPs was determined to be 0.227 nm associated with the (111) plane [46]. This observation aligns with the sized and crystallographic plane indicated by the XRD results, demonstrating consistency. The polydispersity of the biosynthesized AgNPs was calculated to be 0.064% using Equation (2). This result supports successfully synthesizing more uniformly sized and mono-dispersed Ag nanoparticles using mangosteen extract [47].

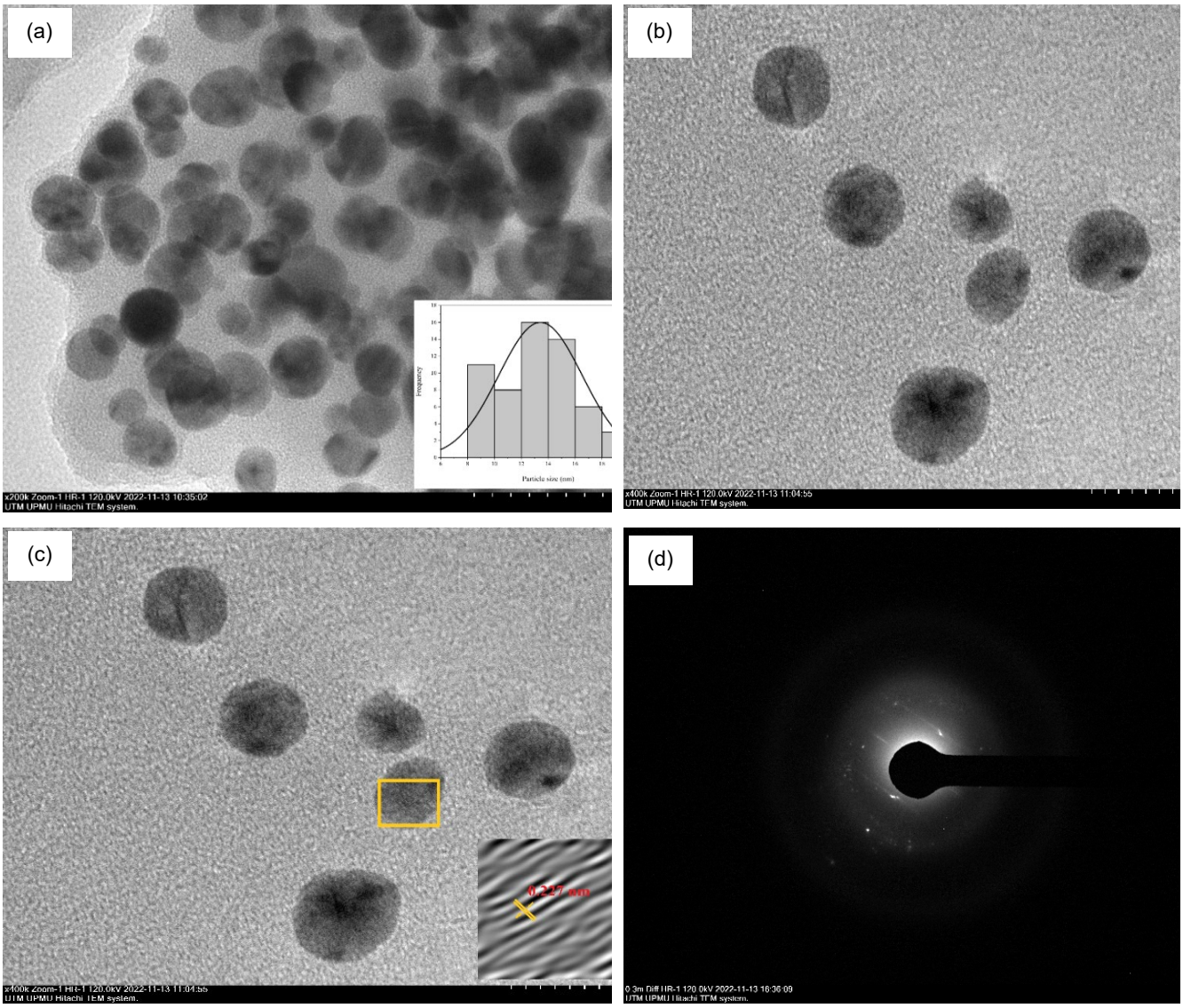

Figure 8. HR-TEM images at selected regions (a) 500 nm with particle size distribution; (b) 300 nm; (c) FFT plot and (d) SAED pattern of biosynthesized AgNPs

Photocatalytic Evaluation on Tetracycline

The photocatalytic activity on tetracycline by the synthesized AgNPs was evaluated once the adsorption-desorption equilibrium was achieved (following a 1 hr interaction period under dark conditions). Self-degradation of tetracycline was conducted to ensure the observed outcomes were not solely attributed to photolysis. The experimental findings indicate that only a minimal portion of tetracycline undergoes degradation when exposed to UV light without a photocatalyst. The photolysis of tetracycline remains relatively stable under UV light, with a 6% degradation rate as illustrated in Figure 9(a). Nevertheless, in the presence of AgNPs, tetracycline exhibits increased instability with approximately 80% of its initial concentration degrading over 4 hrs period. As depicted in Figure 9(a), noticeable degradation begins at 40 min, with 24% of the initial concentration already degraded. This trend continues consistently up to 3 hrs, reaching a degradation percentage of 69%, followed by a gradual decline up to 4 hrs and reaching its equilibrium. In the equilibrium state, all the active sites have been filled with the adsorbed tetracycline molecules. Therefore, extending the experiment will not yield any significant difference. It is noteworthy that tetracycline necessitates higher energy and a longer time for degradation, given its light absorption at lower wavelengths, specifically around 345 and 270 nm [48].

Figure 9(b) illustrates the correlation between ln (A/A_o) and time (min). The analysis revealed adherence to the pseudo-first-order kinetic model that showcases a linear relationship. Simultaneously, the rate constant (k) was calculated using Equation (4). The calculated values were 0.0002 and 0.0066 min^{-1} for the control and Ag photocatalyst, respectively. In comparison, biosynthesized Ag exhibited a kinetic constant 33 times higher than the photolysis in degradation tetracycline at 30 ppm. Numerous studies have been conducted on the degradation of tetracycline involving modification or deposition of silver. However, there is a lack of research specifically focusing on using single AgNPs alone for this purpose. The finding from this study indicates a successful photocatalytic performance in tetracycline degradation using a simple green-synthesized Ag photocatalyst.

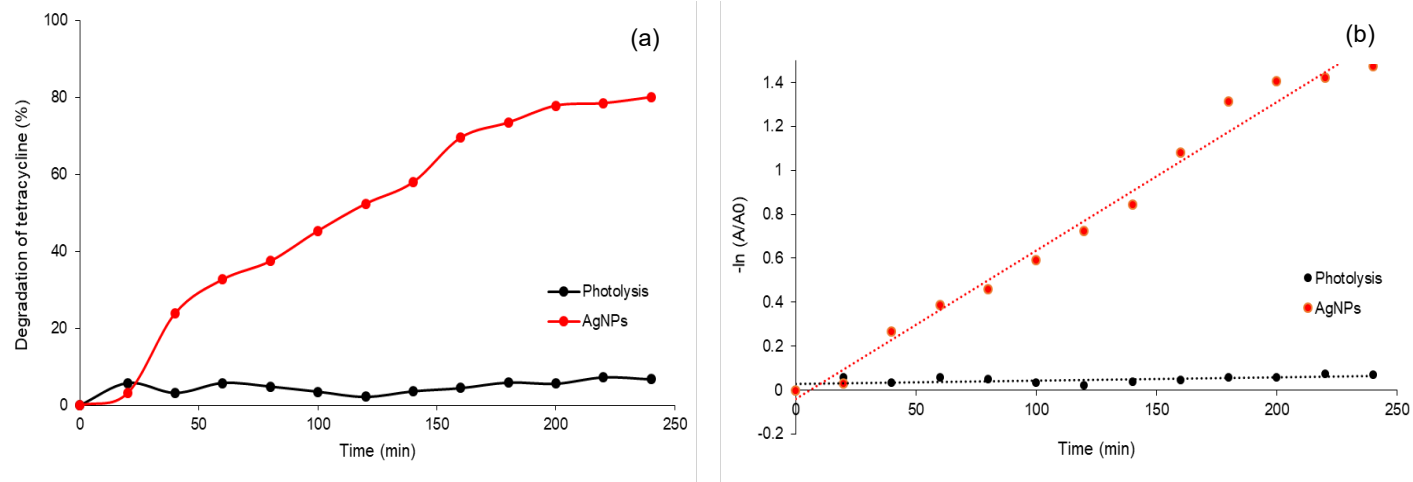

Figure 9. Photocatalytic degradation of tetracycline using biosynthesized AgNPs demonstrated by (a) degradation percentage and (b) kinetic graph

Conclusions

Herein a straightforward and sustainable method utilizes *G. mangostana* pericarp waste as a reducing and stabilizing agent with silver nitrate as a metal precursor to synthesize AgNPs at room temperature. The involvement of α-mangostin in this biosynthesis was proven qualitatively using HPLC. Optimization studies highlighted the significance of the molar ratio GMP:$AgNO_3$ and the pH extract in regulating the synthesis rate, resulting in consistently spherical nanoparticles with crystallite size. The biosynthesized AgNPs exhibited notable effectiveness in tetracycline adsorption under UV light. Furthermore, the AgNPs demonstrated promising potential for application in wastewater management and the pharmaceutical industry. Nevertheless, the biosynthesis approach holds promise for future improvement in a wide range of catalysis reactions and further study is required to validate the durability and mechanism of AgNPs to develop this approach to be greener and more economical.

Conflicts of Interest

The author(s) declare(s) that there is no conflict of interest regarding the publication of this paper.

Acknowledgement

This work is part of a research project, supported by the Ministry of Higher Education, Malaysia from Fundamental research Grant Scheme (FRGS/1/2019/TK10/UTM/02/7) and Universiti Teknologi Malaysia from Geran Penyelidikan Hi-Tech (F4) (Q.J130000.4654.00Q19).

References

[1] Ohiduzzaman, M., Khan, M., Khan, K., & Paul, B. (2024). Biosynthesis of silver nanoparticles by banana pulp extract: Characterizations, antibacterial activity, and bioelectricity generation. *Heliyon, 10*(3), 1–12.

[2] Liu, H., Liu, J., Wang, S., Jin, Z., Ma, R., Zhang, W., Wang, J., Li, J., Song, C., Zhang, S., & Chen, H. (2022). Effect of silver nano-particles and nano-wires on properties of electrically conductive adhesives. *Microelectronics Reliability, 135*, 114571.

[3] Bruna, T., Maldonado-Bravo, F., Jara, P., & Caro, N. (2021). Silver nanoparticles and their antibacterial applications. *International Journal of Molecular Sciences, 22*(13), 1–21.

[4] da Silva, W. L., Druzian, D. M., Oviedo, L. R., Muraro, P., & Oviedo, V. R. (2021). Silver nanoparticles for photocatalysis and biomedical applications. *IntechOpen, 95922*.

[5] Kapoor, R. T., Salvadori, M. R., Rafatullah, M., Siddiqui, M. R., Khan, M. A., & Alshareef, S. A. (2021). Exploration of microbial factories for synthesis of nanoparticles – A sustainable approach for bioremediation of environmental contaminants. *Frontiers in Microbiology, 12*, 658294.

[6] Nam, N. T. H., Linh, N. T. T., Dat, N. M., Bao, P. P., Tinh, N. T., Cong, C. Q., Hai, N. D., Giang, N. T. H., Phong, M. T., & Hieu, N. H. (2023). Applications of highly stable silver nanoparticles from *Garcinia mangostana* pericarp extract: Bioactivities, catalysis, and optical sensing. *Chemistry Select, 8*(38).

[7] Sha, M., Fawcett, D., Sharma, S., Tripathy, S. K., & Poinern, G. E. J. (2015). Green synthesis of metallic nanoparticles via biological entities. *Journal of Materials, 8*(11), 7278–7308.

[8] Hossain, M. A., Paul, B., Khan, K. A., Paul, M., Mamun, M., & Quayum, M. E. (2022). Green synthesis and characterization of silver nanoparticles by using *Bryophyllum pinnatum* and the evaluation of its power generation activities on bio-electrochemical cell. *Material Chemistry and Physics, 282*, 125943.

[9] Hasan, M., Teng, Z., Iqbal, J., Awan, U., Meng, S., Dai, R., Qing, H., & Deng, Y. (2013). Assessment of bioreducing and stabilizing potential of Dragon's Blood (*Dracaena cochinchinensis*, Lour. S. C. Chen) resin extract in synthesis of silver nanoparticles. *Nanoscience and Nanotechnology Letters, 5*(7), 780–784.

[10] Chew, S. Y., Teoh, S. Y., Sim, Y. Y., & Nyam, K. L. (2021). Optimization of ultrasonic extraction condition for maximal antioxidant, antimicrobial, and antityrosinase activity from *Hibiscus cannabinus* L. leaves by using the single factor experiment. *Journal of Applied Research on Medicinal and Aromatic Plants, 25*, 100321.

[11] Nayak, S., Bhat, M. P., Udayashankar, A. C., Laksmeesha, T. R., Geetha, N., & Jogaiah, S. (2020). Biosynthesis and characterization of *Dillenia indica*-mediated silver nanoparticles and their biological activity. *Applied Organometallic Chemistry, 34*(4), 5567.

[12] Chouhan, S., & Guelria, S. (2020). Green synthesis of AgNPs using *Cannabis sativa* leaf extract: Characterization, antibacterial, anti-yeast, and α-amylase inhibitory activity. *Materials Science for Energy Technologies, 3*, 536–544.

[13] Asif, M., Yasmin, R., Ambreen, A., Mustafa, M., & Umbreen, S. (2022). Green synthesis of silver nanoparticles (AgNPs), structural characterization, and their antibacterial potential. *Dose-Response, 20*(2).

[14] Giri, A. K., Jena, B., Biswal, B., Pradhan, A. K., Arakha, M., Acharya, S., & Acharya, L. (2022). Green synthesis and characterization of silver nanoparticles using *Eugenia roxburghii* DC. extract and activity against biofilm-producing bacteria. *Scientific Reports, 12*(1), 1–9.

[15] Obolskiy, D., Pischel, I., Siriwatanametanon, N., & Heinrich, M. (2009). *Garcinia mangostana* L.: A phytochemical and pharmacological review. *Phytotherapy Research, 23*(8), 1047–1065.

[16] Yao, T. L., Nazre, M., Mckey, D., Jalonen, R., & Duminil, J. (2023). The origin of cultivated mangosteen (*Garcinia mangostana* L. var. *mangostana*): Critical assessments and an evolutionary-ecological perspective. *Ecology and Evolution, 13*(3), e9792.

[17] Lin, C. S., Lin, C. L., Ying, T. H., Chiou, H. L., Hung, C. H., Liao, W. S., Hsieh, Y. H., & Kao, S. H. (2020). β-Mangostin inhibits the metastatic power of cervical cancer cells attributing to suppression of JNK2/AP-1/Snail cascade. *Journal of Cellular Physiology, 235*(11), 8446–8460.

[18] Zhou, X., Chen, H., Wei, F., Zhao, Q., Su, Q., Lei, Y., Yin, M., Tian, X., Liu, Z., Yu, B., Bai, C., He, X., & Huang, Z. (2019). α-Mangostin attenuates pristane-induced lupus nephritis by regulating Th17 differentiation. *International Journal of Rheumatic Diseases, 23*(1), 74–83.

[19] Bumrung, J., Chanchao, C., Intasanta, V., Palaga, T., & Wanichwecharungruang, S. (2020). Water-dispersible unadultered α-mangostin particles for biomedical applications. *Royal Society Open Science, 7*(11), 200543.

[20] Li, Q., Yan, X. T., Zhao, L. C., Ren, S., He, Y. F., Liu, W. C., Wang, Z., Li, X. D., Jiang, S., & Li, W. (2020). α-Mangostin, a dietary xanthone, exerts protective effects on cisplatin-induced renal injury via PI3K/Akt and JNK signaling pathways in HEK293 cells. *ACS Omega, 5*(32), 19960–19967.

[21] Masullo, M., Cerulli, A., Cannavacciuolo, C., Kılınç, H., Pizza, C., & Piacente, S. (2022). *Garcinia mangostana* L. fruits and derived food supplements: Identification and quantitative determination of bioactive xanthones by NMR analysis. *Journal of Pharmaceutical and Biomedical Analysis, 218*, 114835.

[22] Govindachari, T., Kalyanaraman, P., Muthukumaraswamy, N., & Pai, B. (1971). Xanthones of *Garcinia mangostana* Linn. *Tetrahedron, 27*(16), 3919–3926.

[23] Valdivia, M. T., Taggart, M., Pap, S., Kean, A., Pfleger, S., & Megson, I. (2023). Photocatalytic metallic nanomaterials immobilized onto porous structures: Future perspectives for at-source pharmaceutical removal from hospital wastewater and potential benefits over existing technologies. *Journal of Water Process Engineering, 52*, 103553.

[24] Scaria, J., Anupama, K. V., & Nidheesh, P. V. (2021). Tetracyclines in the environment: An overview on the occurrence, fate, toxicity, detection, removal methods, and sludge management. *Science of The Total Environment, 771*, 145291.

[25] Wirtz, V. J., Dreser, A., & Gonzales, R. (2010). Trends in antibiotic utilization in eight Latin American countries, 1997–2007. *Revista Panamericana de Salud Pública, 27*(3), 219–225.

[26] Dolan, J. (2003). How much is enough? *LC-GC Europe, 6*, 740–745.

[27] Patra, N., Dehury, N., Pal, A., Behera, A., & Patra, S. (2018). Preparation and mechanistic aspect of natural xanthone functionalized gold nanoparticles. *Materials Science & Engineering C, 90*, 439–445.

[28] Hassan Afandy, H., Sabir, D. K., & Aziz, S. B. (2023). Antibacterial activity of the green synthesized plasmonic silver nanoparticles with crystalline structure against gram-positive and gram-negative bacteria. *Nanomaterials, 13*(8), 1327.

[29] Neethu, S., Midhun, S. J., Sunil, M. A., Soumya, S., Radhakrishnan, E. K., & Jyothis, M. (2018). Efficient visible light induced synthesis of silver nanoparticles by *Penicillium polonicum* ARA 10 isolated from *Chetomorpha antennina* and its antibacterial efficacy against *Salmonella enterica* serovar Typhimurium. *Journal of Photochemistry and Photobiology B: Biology, 180*, 175–185.

[30] Rodríguez-León, E., Iñiguez-Palomares, R., Navarro, R., Herrera-Urbina, R., Tánori, J., Iñiguez-Palomares, C., & Maldonado, A. (2013). Synthesis of silver nanoparticles using reducing agents obtained from natural sources (*Rumex hymenosepalus* extracts). *Nanoscale Research Letters, 8*(1), 1–9.

[31] Aslam, M., Fozia, F., Gul, A., Ahmad, I., Ullah, R., Bari, A., Mothana, R. A., & Hussain, H. (2021). Phyto-extract-mediated synthesis of silver nanoparticles using aqueous extract of *Sanvitalia procumbens* and characterization, optimization, and photocatalytic degradation of azo dyes Orange G and Direct blue-15. *Molecules, 26*(20), 6144.

[32] Handayani, W., Ningrum, A. S., & Imawan, C. (2020). The role of pH in synthesis silver nanoparticles using *Pometia pinnata* (Matoa) leaves extract as bioreductor. *Journal of Physics: Conference Series, 1428*, 012021.

[33] Farrokhnia, M., Karimi, S., & Askarian, S. (2019). Strong hydrogen bonding of gallic acid during synthesis of an efficient AgNPs colorimetric sensor for melamine detection via dis-synthesis strategy. *ACS Sustainable Chemistry & Engineering, 7*(7), 6672–6684.

[34] Davidović, S., Lazić, V., Vukoje, I., Papan, J., Anhrenkiel, S. P., Dimitrijević, S., & Nedeljković, J. M. (2017). Dextran coated silver nanoparticles—Chemical sensor for selective cysteine detection. *Colloids and Surfaces B: Biointerfaces, 160*, 184–191.

[35] Tiwari, H., Samal, K., Geed, S. R., Bera, S., Das, C., & Mohanty, K. (2023). Green synthesis of silver nanoparticles for ultrafiltration membrane surface modification and antimicrobial activity. *Sustainable Chemistry for Climate Action, 3*, 100031.

[36] Alobaid, H. M., Alzhrani, A. H., Majrashi, N. A., Alkhuriji, A. F., Alajmi, R. A., Yehia, H. M., Awad, M. A., Almurshedi, A. S., Almnaizel, A. T., & Elkhadragy, M. F. (2022). Effect of biosynthesized silver nanoparticles by *Garcinia mangostana* extract against human breast cancer cells line MCF-7. *Food Science and Technology, 42*, e102221.

[37] Yoosaf, K., Ipe, B. T., Suresh, C. H., & Thomas, K. G. (2007). In situ synthesis of metal nanoparticles and selective naked-eye detection of lead ions from aqueous media. *The Journal of Physical Chemistry C, 111*(34), 12839–12847.

[38] Khan, M., Khan, A., Rafatullah, M., Mahboob, A., Bogdanchikova, N., & Garibo, D. (2022). Search for effective approaches to fight microorganisms causing high losses in agriculture: Application of *P. lilacinum* metabolites and mycosynthesised silver nanoparticles. *Biomolecules, 12*(2), 174.

[39] Perera, K. M. K. G., Kuruppu, K. A. S. S., Chamara, A. M. R., & Thiripuranathar, G. (2020). Characterization of spherical Ag nanoparticles synthesized from the agricultural wastes of *Garcinia mangostana* and *Nephelium lappaceum* and their applications as a photocatalyzer and fluorescence quencher. *SN Applied Sciences, 2*(12), 1974.

[40] Veerasamy, R., Xin, T. Z., Gunasagaran, S., Wei Xiang, T. F., Chou Yang, E. F., Jeyakumar, N., & Dhanaraj, S. A. (2011). Biosynthesis of silver nanoparticles using mangosteen leaf extract and evaluation of their antimicrobial activities. *Journal of Saudi Chemical Society, 15*(2), 113–120.

[41] Masum, M. M. I., Siddiqa, M. M., Ali, K. A., Zhang, Y., Abdallah, Y., Ibrahim, E., Qiu, W., Yan, C., & Li, B. (2019). Biogenic synthesis of silver nanoparticles using *Phyllanthus emblica* fruit extract and its inhibitory action against the pathogen *Acidovorax oryzae* strain RS-2 of rice bacterial brown stripe. *Frontiers in Microbiology, 10*, 820.

[42] Judy Azar, A. Z., & Mohebbi, S. (2013). One-pot greener synthesis of silver nanoparticles using tangerine peel extract: Large-scale production. *Micro & Nano Letters, 8*(11), 813–815.

[43] Ali, M. H., Kalam Azad, M. A., Khan, K. A., Rahman, M. O., Chakma, U., & Kumer, A. (2023). Analysis of crystallographic structures and properties of silver nanoparticles synthesized using PKL extract and nanoscale characterization techniques. *ACS Omega, 8*(31), 28133–28142.

[44] Alzahrani, E. (2020). Colorimetric detection based on localized surface plasmon resonance optical characteristics for sensing of mercury using green-synthesized silver nanoparticles. *Journal of Analytical Methods in Chemistry, 2020*, 1–12.

[45] Singh, H., Du, J., & Yi, T. H. (2017). *Kinneretia* THG-SQI4 mediated biosynthesis of silver nanoparticles and its antimicrobial efficacy. *Artificial Cells, Nanomedicine, and Biotechnology, 45*(3), 602–608.

[46] Gupta, A., Koirala, A. J., Gupta, B., & Parajuli, N. (2019). Improved method for separation of silver nanoparticles synthesized using the *Nyctanthes arbor-tristis* shrub. *Acta Chemica Malaysia, 3*(1), 35–42.

[47] Fatimah, I., & Aftrid, Z. H. V. I. (2019). Characteristics and antibacterial activity of green synthesized silver nanoparticles using red spinach (*Amaranthus tricolor* L.) leaf extract. *Green Chemistry Letters and Reviews, 12*(1), 25–30.

[48] Olusegun, S. J., Larrea, G., Osial, M., Jackowska, K., & Krysinski, P. (2021). Photocatalytic degradation of antibiotics by superparamagnetic iron oxide nanoparticles. Tetracycline case. *Catalysts, 11*(10), 1243.